IOPscience iopscience.iop.org

Home Search Collections Journals About Contact us My IOPscience

Dressing of ultracold atoms by their Rydberg states in a Ioffe–Pritchard trap

This article has been downloaded from IOPscience. Please scroll down to see the full text article.

2010 J. Phys. B: At. Mol. Opt. Phys. 43 155003

(http://iopscience.iop.org/0953-4075/43/15/155003)

View the table of contents for this issue, or go to the journal homepage for more

Download details:
IP Address: 139.184.30.133
The article was downloaded on 17/10/2012 at 21:02

Please note that terms and conditions apply.

J. Phys. B: At. Mol. Opt. Phys. **43** (2010) 155003 (11pp) doi:10.1088/0953-4075/43/15/155003

Dressing of ultracold atoms by their Rydberg states in a Ioffe–Pritchard trap

Michael Mayle[1], **Igor Lesanovsky**[2] **and Peter Schmelcher**[1]

[1] Zentrum für Optische Quantentechnologien, Universität Hamburg, Luruper Chaussee 149, 22761 Hamburg, Germany
[2] Midlands Ultracold Atom Research Centre-MUARC, The University of Nottingham, School of Physics and Astronomy, Nottingham, UK

E-mail: michael.mayle@physnet.uni-hamburg.de

Received 12 February 2010, in final form 26 May 2010
Published 7 July 2010
Online at stacks.iop.org/JPhysB/43/155003

Abstract
We explore how the extraordinary properties of Rydberg atoms can be employed to impact the motion of ultracold ground state atoms. Specifically, we use an off-resonant two-photon laser dressing to map features of the Rydberg states on ground state atoms. It is demonstrated that the interplay between the spatially varying quantization axis of the considered Ioffe–Pritchard field and the fixed polarizations of the laser transitions provides the possibility of substantially manipulating the ground state trapping potential.

(Some figures in this article are in colour only in the electronic version)

1. Introduction

Rydberg atoms are—amongst others—highly susceptible to external fields and show a strong mutual interaction [1]. Combining the extraordinary properties of Rydberg atoms, which originate from the large displacement of the valence electron and the remaining ionic core, with the plethora of techniques known from the preparation and manipulation of ultracold gases enables remarkable observations such as the excitation blockade between two single atoms a few μm apart [2, 3]. Moreover, interacting Rydberg atoms serve as flexible tools for various purposes. For example, their strong dipole–dipole interaction renders Rydberg atoms interesting candidates for the realization of two-qubit quantum gates [4, 5] or efficient multiparticle entanglement [6–8]. In fact, only very recently a CNOT gate between two individually addressed neutral atoms and the generation of entanglement has been experimentally demonstrated by employing the Rydberg blockade mechanism [9, 10].

Other proposals utilize the peculiar properties of an ensemble of interacting Rydberg atoms by employing an off-resonant laser coupling that dresses ground state atoms with Rydberg states. For example, a method has been proposed of creating a polarized atomic dipolar gas by coupling to an electrically polarized Rydberg state [11]. The resulting long-ranged dipole–dipole interaction in such gases are predicted to give rise to dipolar crystals and novel supersolid phases [12, 13]. In a similar manner, the Rydberg dressing of ground state atoms is expected to entail a roton–maxon excitation spectrum in three-dimensional Bose–Einstein condensates [14] and collective many-body interactions [15]. Here, we discuss a further application for the use of Rydberg states, namely, how they can be employed for substantially manipulating the trapping potentials of magnetically trapped ^{87}Rb atoms in a controlled manner.

Inhomogeneous magnetic trapping fields are omnipresent in experiments dealing with ultracold atoms. Constituting a promising alternative to optical approaches, even one- and two-dimensional lattices of magnetic microtraps have been realized experimentally [16–19]. The issue of trapping Rydberg atoms in magnetic traps—primarily of Ioffe–Pritchard kind—has been studied extensively, demonstrating that Rydberg atoms can be tightly confined [20, 21] and that one-dimensional Rydberg gases can be created and stabilized by means of an additional electric field [22]. In particular, the authors demonstrated in a previous work that the trapping potentials of ^{87}Rb Rydberg atoms in low angular momentum electronic states (i.e. $l \leqslant 2$) considerably deviate from the behaviour known from ground state atoms [23]. This effect is due to the *composite* nature of Rydberg atoms, i.e. the fact that they consist of an outer valence electron far apart from the ionic core.

In the present work we demonstrate how the peculiar properties of the Rydberg trapping potential can be utilized

 © 2010 IOP Publishing Ltd Printed in the UK & the USA

to manipulate the trapping potential for the ground state. To this end, an off-resonant two-photon laser transition is employed that dresses the ground state atoms by their Rydberg states. We thoroughly discuss the coupling scheme previously employed in [24] and systematically study the resulting dressed potentials. In particular, it is demonstrated how the delicate interplay between the spatially varying quantization axis of the Ioffe–Pritchard field and the fixed polarizations of the laser transitions greatly influences the actual shape of the trapping potentials—a mechanism that has been employed also very recently to create versatile atom traps by means of a Raman-type setup [25]. Moreover, the employed scheme allows us to map the Rydberg trapping potential onto the ground state.

In detail, we proceed as follows. Section 2 briefly reviews the properties of Rydberg atoms in a magnetic Ioffe–Pritchard trap as derived in [23]; the resulting trapping potentials are contrasted with the ones belonging to ground state atoms. Section 3 then introduces the off-resonant two-photon laser coupling scheme that dresses the ground state with the Rydberg state. In section 4 we establish a simplified three-level scheme (opposed to the 32-level scheme that is needed to fully describe the excitation dynamics) that allows us to derive analytical expressions of the dressed potentials. Section 5 contains a thorough discussion of the dressed ground trapping potentials for a variety of field and laser configurations.

2. Review of the Rydberg trapping potentials

Let us start by briefly recapitulating the results from [23] concerning the trapping potentials of alkali Rydberg atoms in their nS, nP and nD electronic states. As the basic ingredient for magnetically trapping Rydberg atoms, we consider the Ioffe–Pritchard field configuration given by $\mathbf{B}(\mathbf{x}) = \mathbf{B}_c + \mathbf{B}_l(\mathbf{x})$ with $\mathbf{B}_c = B\mathbf{e}_3$, $\mathbf{B}_l(\mathbf{x}) = G\,[x_1\mathbf{e}_1 - x_2\mathbf{e}_2]$. The corresponding vector potential reads $\mathbf{A}(\mathbf{x}) = \mathbf{A}_c(\mathbf{x}) + \mathbf{A}_l(\mathbf{x})$, with $\mathbf{A}_c(\mathbf{x}) = \frac{B}{2}[x_1\mathbf{e}_2 - x_2\mathbf{e}_1]$ and $\mathbf{A}_l(\mathbf{x}) = Gx_1x_2\mathbf{e}_3$; B and G are the Ioffe field strength and the gradient, respectively. The mutual interaction of the highly excited valence electron and the remaining closed-shell ionic core of a Rydberg atom is modelled by an effective potential which depends only on the distance of the two particles. After introducing relative and centre of mass coordinates ($\mathbf{r}$ and $\mathbf{R}$) and employing the unitary transformation $U = \exp\left[\frac{\mathrm{i}}{2}(\mathbf{B}_c \times \mathbf{r}) \cdot \mathbf{R}\right]$, the Hamiltonian describing the Rydberg atom becomes (atomic units are used unless stated otherwise)

$$H = H_A + \frac{\mathbf{P}^2}{2M} + \frac{1}{2}[\mathbf{L} + 2\mathbf{S}] \cdot \mathbf{B}_c + \mathbf{S} \cdot \mathbf{B}_l(\mathbf{R} + \mathbf{r}) + \mathbf{A}_l(\mathbf{R} + \mathbf{r}) \cdot \mathbf{p} + H_{\mathrm{corr}}. \tag{1}$$

Here, $H_A = \mathbf{p}^2/2 + V_l(r) + V_{\mathrm{so}}(\mathbf{L}, \mathbf{S})$ is the field-free Hamiltonian of the valence electron whose core penetration, scattering and polarization effects are accounted for by the l-dependent model potential $V_l(r)$ [26] while $\mathbf{L}$ and $\mathbf{S}$ denote its orbital angular momentum and spin, respectively. $V_{\mathrm{so}}(\mathbf{L}, \mathbf{S}) = \frac{\alpha^2}{2}\left[1 - \frac{\alpha^2}{2}V_l(r)\right]^{-2}\frac{1}{r}\frac{\mathrm{d}V_l(r)}{\mathrm{d}r}\mathbf{L} \cdot \mathbf{S}$ denotes the spin–orbit interaction that couples $\mathbf{L}$ and $\mathbf{S}$ to the total electronic angular momentum $\mathbf{J} = \mathbf{L} + \mathbf{S}$; the term $[1 - \alpha^2 V_l(r)/2]^{-2}$ has been introduced to regularize the nonphysical divergence near the origin [27]. $H_{\mathrm{corr}} = -\boldsymbol{\mu}_c \cdot \mathbf{B}(\mathbf{R}) + \frac{1}{2}\mathbf{A}_c(\mathbf{r})^2 + \frac{1}{2}\mathbf{A}_l(\mathbf{R} + \mathbf{r})^2 + \frac{1}{M}\mathbf{B}_c \cdot (\mathbf{r} \times \mathbf{P}) + U^\dagger[V_l(r) + V_{\mathrm{so}}(\mathbf{L}, \mathbf{S})]U - V_l(r) - V_{\mathrm{so}}(\mathbf{L}, \mathbf{S})$ are small corrections that are neglected in the parameter regime we are focusing on; the magnetic moment of the ionic core is connected to the nuclear spin $\mathbf{I}$ according to $\boldsymbol{\mu}_c = -\frac{1}{2}g_I\mathbf{I}$, with g_I being the nuclear g-factor. In order to solve the resulting coupled Schrödinger equation, we employ a Born–Oppenheimer separation of the centre of mass motion and the electronic degrees of freedom. We are thereby led to an electronic Hamiltonian for the fixed centre of mass position of the atom whose eigenvalues $E_\kappa(\mathbf{R})$ depend parametrically on the centre of mass coordinates. These adiabatic electronic surfaces serve as trapping potentials for the quantized centre of mass motion.

For the fixed total electronic angular momentum $\mathbf{J} = \mathbf{L} + \mathbf{S}$, approximate expressions for the adiabatic electronic energy surfaces can be derived by applying the spatially dependent transformation $U_r = \mathrm{e}^{-\mathrm{i}\gamma(L_x+S_x)}\,\mathrm{e}^{-\mathrm{i}\beta(L_y+S_y)}$ that rotates the local magnetic field vector into the z-direction of the laboratory frame of reference. The corresponding rotation angles are defined by $\sin\gamma = -GY/\sqrt{B^2 + G^2(X^2 + Y^2)}$, $\sin\beta = -GX/\sqrt{B^2 + G^2X^2}$, $\cos\gamma = \sqrt{B^2 + G^2X^2}/\sqrt{B^2 + G^2(X^2 + Y^2)}$ and $\cos\beta = B/\sqrt{B^2 + G^2X^2}$. In second-order perturbation theory, the adiabatic electronic energy surfaces read

$$E_\kappa(\mathbf{R}) = E_\kappa^{(0)}(\mathbf{R}) + E_\kappa^{(2)}(\mathbf{R}), \tag{2}$$

where

$$E_\kappa^{(0)}(\mathbf{R}) = E_\kappa^{\mathrm{el}} + \tfrac{1}{2}g_j m_j\sqrt{B^2 + G^2(X^2 + Y^2)} \tag{3}$$

represents the coupling of a point-like particle to the magnetic field via its magnetic moment $\boldsymbol{\mu} \propto \mathbf{J} = \mathbf{L} + \mathbf{S}$; κ represents the electronic state under investigation, i.e. $|\kappa\rangle = |njm_jls\rangle$, $g_j = \frac{3}{2} + \frac{s(s+1)-l(l+1)}{2j(j+1)}$ is its Landé g-factor and E_κ^{el} is the field-free atomic energy levels. $E_\kappa^{(0)}(\mathbf{R})$ is rotationally symmetric around the Z-axis and confining for $m_j > 0$. For small radii ($\rho = \sqrt{X^2 + Y^2} \ll B/G$) an expansion up to second order yields a harmonic potential

$$E_\kappa^{(0)}(\rho) \approx E_\kappa^{\mathrm{el}} + \tfrac{1}{2}g_j m_j B + \tfrac{1}{2}M\omega^2\rho^2 \tag{4}$$

with the trap frequency defined by $\omega = G\sqrt{\frac{g_j m_j}{2MB}}$ while we find a linear behaviour $E_\kappa^{(0)}(\rho) \approx E_\kappa^{el} + \frac{1}{2}g_j m_j G\rho$ when the centre of mass is far from the Z-axis ($\rho \gg B/G$).

The second-order contribution $E_\kappa^{(2)}(\mathbf{R})$ stems from the composite nature of the Rydberg atom, i.e. the fact that it consists of an outer Rydberg electron far apart from the ionic core. It reads

$$E_\kappa^{(2)}(\mathbf{R}) = CG^2X^2Y^2, \tag{5}$$

where the coefficient C depends on the electronic state κ under investigation. Since C is generally negative [23], a deconfining behaviour of the energy surface for large centre of mass coordinates close to the diagonal ($X = Y$) is found. For a detailed derivation and discussion of the Rydberg trapping potentials (2)–(5), we refer the reader to [23].

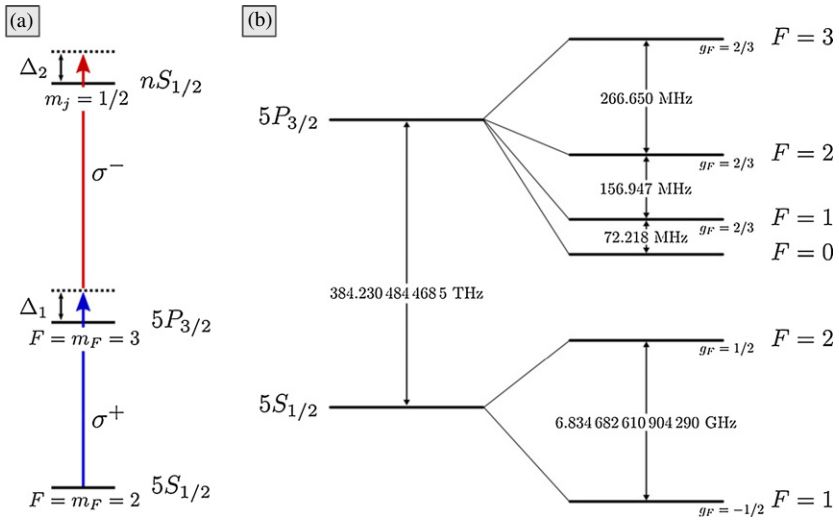

Figure 1. (a) Idealized level scheme for an off-resonant two-photon coupling of the ground state and Rydberg state of ^{87}Rb. In a Ioffe–Pritchard trap, additional atomic levels and polarizations contribute away from the trap centre, see the text. Note that the hyperfine splittings of the Rydberg level are included in the calculation although not shown in this figure. (b) Atomic energy level scheme of the $5S_{1/2}$ and $5P_{3/2}$ states of ^{87}Rb including the hyperfine splittings.

2.1. Trapping potentials of ground-state atoms

When considering the trapping of ground-state atoms, the coupling mechanism relies on the point-like interaction of the atomic magnetic moment $\boldsymbol{\mu}$ with the external field. Since the hyperfine interaction easily overcomes the Zeeman splitting for the regime of magnetic field strengths we are interested in, we include the hyperfine interaction in our theoretical considerations and assume the atom to couple via its total angular momentum $\boldsymbol{\mu} \propto \mathbf{F} = \mathbf{J} + \mathbf{I}$ to the magnetic field ($\mathbf{I}$ being the nuclear spin). The ground state trapping potentials correspondingly read

$$E_\kappa(\mathbf{R}) = E_\kappa^{\mathrm{el}} + \tfrac{1}{2} g_F m_F |\mathbf{B}(\mathbf{R})|, \tag{6}$$

where E_κ^{el} includes the hyperfine as well as spin–orbit effects, and

$$g_F = g_j \frac{F(F+1) + j(j+1) - I(I+1)}{2F(F+1)}. \tag{7}$$

Let us note that for Rydberg atoms the hyperfine interaction $H_{\mathrm{hfs}} = A\mathbf{I}\cdot\mathbf{J}$ only plays a minor role since the hyperfine constant A scales as n^{-3} [28]. For a wide range of field strengths it is therefore sufficient to treat the hyperfine interaction perturbatively, giving rise to a mere splitting of the Rydberg trapping potentials (2) according to $W_{\mathrm{hfs}} = A m_i m_j$ [29]. Correspondingly, we continue to label the Rydberg states by their j, m_j and m_I quantum numbers rather than the F, m_F ones. In particular, for characterizing the Rydberg trapping potentials the j, m_j quantum numbers are sufficient. In our numerical calculations, on the other hand, we fully incorporated the hyperfine interaction H_{hfs} of the Rydberg state. Moreover, we also included the coupling of the magnetic moment of the ionic core, $\boldsymbol{\mu} \propto \mathbf{I}$, to the field. Finally, we remark that—except for the electronic energy offset E_κ^{el}—the zeroth-order Rydberg trapping potential $E^{(0)}_{n\mathrm{S}_{1/2},m_j=1/2}(\mathbf{R})$ and the $5\mathrm{S}_{1/2}$ ground state energy surface are identical for $F = m_F = 2$.

3. Off-resonant coupling scheme

In this section, we discuss the coupling scheme of the ground state and Rydberg state that arises for a two-photon off-resonant laser excitation in the presence of the Ioffe–Pritchard trap. The off-resonant coupling results in a dressed ground state atom to which the Rydberg state is weakly admixed. In this manner, the ground state atom gains properties that are specific for the Rydberg atom. In particular, the peculiar properties of the Rydberg trapping surfaces can be exploited for substantially manipulating the trapping potentials of ground state atoms.

We investigate the excitation scheme that is frequently encountered in experiments [30, 31]: laser 1, which is σ^+ polarized, drives the transition s $\rightarrow$ p detuned by Δ_1 while a second, σ^- polarized laser then couples to the Rydberg state $n \equiv n\mathrm{S}_{1/2}, m_j = 1/2, m_I = 3/2$, with s denoting the ground state $5\mathrm{S}_{1/2}$, $F = m_F = 2$ and p the intermediate state $5\mathrm{P}_{3/2}$, $F = m_F = 3$. Both lasers are propagating along the $\mathbf{e}_3$-axis in the laboratory frame of reference; the complete two-photon transition is supposed to be off-resonant by Δ_2. A sketch of the whole scheme is provided in figure 1(a). In a Ioffe–Pritchard trap, however, the quantization axis is spatially dependent and the polarization vectors of the two excitation lasers are only well defined as σ^+ and σ^- at the trap centre. As we are going to show in the following, in the rotated frame of reference, i.e. after applying the unitary transformation U_r, contributions of all polarizations emerge and the excitation scheme becomes more involved.

In the dipole approximation, the interaction of the atom with the laser fields is given by

$$H_{\mathrm{AF}} = -\sum_{i=1}^{2} \mathbf{d}\cdot\mathbf{E}_i(t) = \sum_{i=1}^{2} \mathbf{r}\cdot\mathbf{E}_i(t), \tag{8}$$

where the sum runs over the two applied excitation lasers. The electric field vectors $\mathbf{E}_i(t)$ can be decomposed into

their positive- and negative-rotating components according to $\mathbf{E}_i^{(+)}(t)$ and $\mathbf{E}_i^{(-)}(t)$,

$$\mathbf{E}_i(t) = \frac{E_{i0}}{2}(\boldsymbol{\epsilon}_i\, \mathrm{e}^{-\mathrm{i}\omega t} + \boldsymbol{\epsilon}_i^*\, \mathrm{e}^{\mathrm{i}\omega t}) \tag{9}$$

$$\equiv \mathbf{E}_i^{(+)}(t) + \mathbf{E}_i^{(-)}(t), \tag{10}$$

i.e. $\mathbf{E}_i^{(\pm)} \propto \mathrm{e}^{-\mathrm{i}(\pm\omega)t}$. The electric field amplitude E_{i0} is connected to the intensity I_i of the ith laser via $E_{i0} = \sqrt{2I_i/c\varepsilon_0}$. We distinguish three different polarization vectors $\boldsymbol{\epsilon}$ of the excitation lasers, namely, $\boldsymbol{\epsilon}_\pm = (\mathbf{e}_1 \pm \mathrm{i}\mathbf{e}_2)/\sqrt{2}$ and $\boldsymbol{\epsilon}_0 = \mathbf{e}_3$ for $\sigma^\pm$- and π-polarized light, respectively.

In order to solve the time-dependent Schrödinger equation, the Hamiltonian for the atom in the Ioffe–Pritchard trap and the laser interaction must be expressed in the same frame of reference. Hence, the unitary transformations of the previous section must be applied to H_{AF} as well. The first one, $U = \exp\left\{\frac{\mathrm{i}}{2}(\mathbf{B}_c \times \mathbf{r}) \cdot \mathbf{R}\right\}$, leaves the interaction Hamiltonian (8) of the atom with the lasers unchanged. The transformation $U_r = \mathrm{e}^{-\mathrm{i}\gamma J_x}\, \mathrm{e}^{-\mathrm{i}\beta J_y}$ into the rotated frame of reference, on the other hand, yields

$$U_r\, \mathbf{r} U_r^\dagger = \begin{pmatrix} x\cos\beta + y\sin\gamma\sin\beta - z\cos\gamma\sin\beta \\ y\cos\gamma + z\sin\gamma \\ x\sin\beta - y\sin\gamma\cos\beta + z\cos\gamma\cos\beta \end{pmatrix}. \tag{11}$$

That is, the σ^+ and σ^- laser transitions that are depicted in figure 1(a) become

$$\boldsymbol{\epsilon}_\pm \cdot U_r \mathbf{r} U_r^\dagger = \frac{1}{\sqrt{2}}[x\cos\beta + y\sin\gamma\sin\beta - z\cos\gamma\sin\beta \pm \mathrm{i}(y\cos\gamma + z\sin\gamma)]. \tag{12}$$

Equation (12) can be rewritten in terms of the polarization vectors $\tilde{\boldsymbol{\epsilon}}_\pm$ and $\tilde{\boldsymbol{\epsilon}}_0$ defined in the rotated frame of reference. To this end, we rotate the polarization vector $\boldsymbol{\epsilon}$ and leave the position operator $\mathbf{r}$ unchanged: $\boldsymbol{\epsilon} \cdot U_r \mathbf{r} U_r^\dagger \to (\mathcal{R}\boldsymbol{\epsilon}) \cdot \mathbf{r}$ with $\mathcal{R}$ denoting the rotation matrix associated with the transformation U_r. $\mathcal{R}\boldsymbol{\epsilon}$ can then be decomposed into the components $\tilde{\boldsymbol{\epsilon}}_\pm$ and $\tilde{\boldsymbol{\epsilon}}_0$, i.e. $\mathcal{R}\boldsymbol{\epsilon} = \sum_{i=\pm,0} c_i \tilde{\boldsymbol{\epsilon}}_i$ with $c_i = \tilde{\boldsymbol{\epsilon}}_i^* \cdot \mathcal{R}\boldsymbol{\epsilon}$. Employing

$$\mathcal{R}\boldsymbol{\epsilon}_\pm = \frac{1}{\sqrt{2}} \begin{pmatrix} \cos\beta \\ \sin\gamma\sin\beta \pm \mathrm{i}\cos\gamma \\ -\cos\gamma\sin\beta \pm \mathrm{i}\sin\gamma \end{pmatrix} \tag{13}$$

finally yields

$$\boldsymbol{\epsilon}_+ \cdot U_r \mathbf{r} U_r^\dagger = \left[\tfrac{1}{2}(\cos\gamma + \cos\beta - \mathrm{i}\sin\gamma\sin\beta)\tilde{\boldsymbol{\epsilon}}_+ - \tfrac{1}{2}(\cos\gamma - \cos\beta - \mathrm{i}\sin\gamma\sin\beta)\tilde{\boldsymbol{\epsilon}}_- - \tfrac{1}{\sqrt{2}}(\cos\gamma\sin\beta - \mathrm{i}\sin\gamma)\tilde{\boldsymbol{\epsilon}}_0\right] \cdot \mathbf{r}, \tag{14}$$

$$\boldsymbol{\epsilon}_- \cdot U_r\, \mathbf{r} U_r^\dagger = \left(\boldsymbol{\epsilon}_+ \cdot U_r \mathbf{r} U_r^\dagger\right)^*. \tag{15}$$

Thus, in the rotated frame of reference contributions of all polarizations emerge away from the trap centre. In particular, the $5S_{1/2}$, $F = m_F = 2$ ground state can also couple to $m_F < 3$ magnetic sublevels of the $5P_{3/2}$ intermediate state. Moreover, two-photon couplings between the $5S_{1/2}$, $F = m_F = 2$ and $5S_{1/2}$, $F = 2, m_F < 2$ levels via the hyperfine levels of the $5P_{3/2}$ intermediate state emerge if the first excitation laser gains a significant contribution of the σ^-- or π-polarization in the rotated frame of reference. On the Rydberg side, also $m_j = -1/2$ states become accessible. As a results, the simple three-level excitation scheme s $\leftrightarrow$ p $\leftrightarrow$ n is in general not sufficient and all relevant hyperfine levels must be included in the theoretical treatment. In detail, these are the $F = 1$ and $F = 2$ hyperfine levels of the $5S_{1/2}$ ground and the $nS_{1/2}$ Rydberg state. For the intermediate $5P_{3/2}$ state, we have $F \in \{0, 1, 2, 3\}$. Of course, for each F there are in addition $2F + 1$ magnetic sublevels with $|m_F| \leqslant F$. Note that the intermediate $5P_{3/2}$, $F < 3$ states are split considerably below the $5P_{3/2}$, $F = 3$ levels because of the hyperfine interaction, see figure 1(b). An even stronger splitting is encountered for the $F = 1$ and $F = 2$ hyperfine levels of the $5S_{1/2}$ electronic state. Nevertheless, all these states are taken into account in our numerical calculations, yielding in total 32 states. Other electronic states are far off-resonant and thus do not contribute in the excitation dynamics.

The resulting multi-level excitation scheme is solved by employing the rotating wave approximation while adiabatically eliminating the intermediate states by a strong off-resonance condition. This procedure results in an effective coupling matrix for the ground and Rydberg states whose diagonalization yields a dressed electronic potential energy surface for the centre of mass motion of the ground state atom. In the next section, we derive the coupling matrix for the illustrative example of a simplified three-level system. The generalization to the full level scheme is straightforward, although laborious.

4. Simplified three-level scheme

In this section, we restrict ourselves to the three-level system s $\leftrightarrow$ p $\leftrightarrow$ n, i.e. including from the transformed dipole interaction (14)–(15) only the σ^+ and σ^- part for the first and second laser, respectively. Such a simplification allows us to derive analytical solutions of the time-dependent Schrödinger equation and therefore constitutes a particularly illustrative example. It is expected to be valid for large Ioffe fields B and/or small gradients G when the quantization axis only shows a weak spatial dependence and the $nS_{1/2}, m_j = 1/2, m_I = 3/2$ Rydberg state is predominantly addressed via the $5P_{3/2}$, $F = m_F = 3$ intermediate state. For higher gradients, the polarization vector significantly changes its character throughout the excitation area such that the contributions of other states can no longer be neglected.

The three-level system can be further simplified by adiabatically eliminating the intermediate state p by a strong off-resonance condition, i.e. assuming $|\Delta_1| \gg \omega_{\mathrm{ps}}$ and $|\Delta_1 - \Delta_2| \gg \omega_{\mathrm{np}}$ with ω_{ps} and ω_{np} being the single-photon Rabi frequencies of the first and second laser transitions, respectively:

$$\omega_{\mathrm{ps}} = \tfrac{1}{2}(\cos\gamma + \cos\beta - \mathrm{i}\sin\gamma\sin\beta) \cdot \omega_{\mathrm{ps}}^{(0)} = \omega_{\mathrm{sp}}^*, \tag{16}$$

$$\omega_{\mathrm{np}} = \tfrac{1}{2}(\cos\gamma + \cos\beta + \mathrm{i}\sin\gamma\sin\beta) \cdot \omega_{\mathrm{np}}^{(0)} = \omega_{\mathrm{pn}}^*. \tag{17}$$

Here $\omega_{\mathrm{ps}}^{(0)} = E_{1,0}\langle p|\tilde{\boldsymbol{\epsilon}}_+ \cdot \mathbf{r}|s\rangle$ and $\omega_{\mathrm{np}}^{(0)} = E_{2,0}\langle n|\tilde{\boldsymbol{\epsilon}}_- \cdot \mathbf{r}|p\rangle$ denote the single-photon Rabi frequencies at the trap centre. We remark that in the regime of strong Ioffe fields, where the simplified three-level scheme is valid, the spatial dependences

of (16)–(17) are largely negligible. Hence, the single-photon Rabi frequencies are to a good approximation given by their values $\omega_{\rm ps}^{(0)}$ and $\omega_{\rm np}^{(0)}$ at the origin. Employing in addition the rotating wave approximation, quasidegenerate van Vleck perturbation theory [32] provides us an effective two-level Hamiltonian for the ground state s and the Rydberg state n:

$$\mathcal{H}_{2l} = \begin{pmatrix} \Delta_2 + \tilde{E}_n + E_{\rm hfs} + V_n & \Omega/2 \\ \Omega^*/2 & \tilde{E}_s + V_s \end{pmatrix}. \tag{18}$$

Here, $E_{\rm hfs}$ includes the energy shift due to the hyperfine splitting of the Rydberg state as well as the Zeeman shift of the nuclear spin. For a detailed derivation of Hamiltonian (18), we refer the reader to the appendix of this work. $\tilde{E}_n \equiv \frac{1}{2}|\mathbf{B}(\mathbf{R})| + C \cdot G^2 X^2 Y^2$, $\tilde{E}_s \equiv \frac{1}{2}|\mathbf{B}(\mathbf{R})|$ and $\tilde{E}_p \equiv |\mathbf{B}(\mathbf{R})|$ are the trapping potentials of the individual energy levels. Note that the Rydberg state n experiences the same potential energy surface as the ground state s, plus the perturbation $E^{(2)}_{n{\rm S}_{1/2}}(\mathbf{R})$ due to its non-point-like character. The laser detunings are defined by $\Delta_1 = E_p^{\rm el} - E_s^{\rm el} - \omega_1$ and $\Delta_2 = E_n^{\rm el} - E_s^{\rm el} - \omega_1 - \omega_2$. The effective interaction between the ground state and Rydberg state is given by the two-photon Rabi frequency:

$$\Omega = \frac{\omega_{\rm ps}\omega_{\rm np}}{4}\left[\frac{1}{\tilde{E}_s - \tilde{E}_p - \Delta_1} + \frac{1}{\tilde{E}_n - \tilde{E}_p + \Delta_2 - \Delta_1 + E_{\rm hfs}}\right]. \tag{19}$$

On the diagonal of Hamiltonian (18) we find the contributions

$$V_n = -\frac{1}{4}\frac{|\omega_{\rm np}|^2}{\tilde{E}_p - \tilde{E}_n + \Delta_1 - \Delta_2 - E_{\rm hfs}}, \tag{20}$$

$$V_s = -\frac{1}{4}\frac{|\omega_{\rm ps}|^2}{\tilde{E}_p - \tilde{E}_s + \Delta_1}, \tag{21}$$

which are the light shifts of the Rydberg state and ground state, respectively. In the limit $\Delta_1 \gg \Delta_2$ and neglecting the energy surfaces $\tilde{E}_i$—which means looking at the trap centre—one recovers $\Omega = -\omega_{\rm ps}\omega_{\rm np}/2\Delta_1$, $V_n = -|\omega_{\rm np}|^2/4\Delta_1$ and $V_s = -|\omega_{\rm ps}|^2/4\Delta_1$.

The diagonalization of Hamiltonian (18) yields the *dressed* Rydberg (+) and ground state energy surfaces (−),

$$E_\pm(\mathbf{R}) = \frac{1}{2}\Big[\tilde{E}_s + V_s + \tilde{E}_n + V_n + \Delta_2 + E_{\rm hfs} \pm \sqrt{(\tilde{E}_n + V_n - \tilde{E}_s - V_s + \Delta_2 + E_{\rm hfs})^2 + \Omega^2}\Big], \tag{22}$$

that serve as the trapping potential for the external motion. Here, we are mainly interested in the dressed potential for the ground state. For large detunings $\Delta_2 \gg \Omega$ one can approximate

$$E_-(\mathbf{R}) \approx \tilde{E}_s + V_s - \frac{\Omega^2}{4\Delta_2} + \frac{\Omega^2}{4\Delta_2^2}(\tilde{E}_n + V_n - \tilde{E}_s - V_s), \tag{23}$$

i.e. the contribution of the Rydberg surface $\tilde{E}_n$ to the dressed ground state trapping potential $E_-(\mathbf{R})$ is suppressed by the factor $(\Omega/\Delta_2)^2$. Note that any spatial variation in the light shift V_s and in the Rabi frequency Ω will effectively alter the trapping potential experienced by the dressed ground state atom.

5. Dressed ground state trapping potentials

In this section, we investigate the dressed ground state trapping potentials arising from the two-photon coupling described in section 3. Since the actual shape of these energy surfaces is determined by the interplay of the various parameters belonging to the field configuration (B and G) as well as to the laser couplings $\left(\omega_{\rm ps}^{(0)}, \omega_{\rm np}^{(0)}, \Delta_1 \text{ and } \Delta_2\right)$, there is a plethora of possible configurations. Nevertheless, one can distinguish basically two relevant regimes based on the magnetic field parameters. First of all, there is the regime where the ground state trapping potential is substantially influenced by the admixture of the Rydberg surface. This regime is usually encountered for a Ioffe dominated magnetic field configuration combined with a relatively strong laser coupling. In contrast, the second regime is obtained for strong gradient fields. In this case, the resulting spatially inhomogeneous light shift determines the characteristics of the ground state trapping potential and the contribution of the Rydberg surface is of minor importance. Exemplary dressed energy surfaces belonging to both regimes are discussed in the following. We stress that for determining the dressed trapping potentials the full 32-level scheme is solved. Comparisons with the analytically obtained result (22) are provided. Concerning the choice of the Rydberg state n, a principal quantum number of $n = 40$ is considered throughout this section.

5.1. Dressed trapping potentials of the $m_F = 2$ state

Let us start by investigating the dressed potential arising for the $5{\rm S}_{1/2}$, $m_F = 2$ state of the rubidium atom. As mentioned before, in zero order this state gives rise to the same trapping potential as the $n{\rm S}_{1/2}$ Rydberg state. Hence, when going from the non-dressed to the dressed potential, any changes that arise can be mapped directly to either the higher order properties of the Rydberg trapping potential or the influence of a spatially dependent light shift.

In figures 2(a) and (b) the trapping potential of the dressed ground state atom is illustrated for the configuration $B = 25\,{\rm G}$, $G = 2.5\,{\rm Tm}^{-1}$, $\omega_{\rm ps}^{(0)} = 2\pi \times 100\,{\rm MHz}$, $\omega_{\rm np}^{(0)} = 2\pi \times 130\,{\rm MHz}$, $\Delta_1 = -2\pi \times 40\,{\rm GHz}$ and $\Delta_2 = -2\pi \times 1.5\,{\rm MHz}$. In this strongly Ioffe field dominated case, the contribution $E^{(2)}_{40{\rm S}}(\mathbf{R})$ to the Rydberg trapping potential $E_{40{\rm S}}(\mathbf{R})$ is very strong, cf (2). As a result, the Rydberg potential energy surface is extremely shallow and does not confine even a single centre of mass state [23]. According to (23), this strong deviation from the harmonic confinement of the ground state, $E_{5{\rm S}}(\mathbf{R}) \propto \frac{1}{2}M\omega^2\rho^2$, is consequently mirrored in the dressed ground state potential: along the diagonal ($X = Y$), where the effect of $E^{(2)}_{40{\rm S}}(\mathbf{R})$ is most pronounced, the trapping potential is gradually lowered compared to the harmonic confinement of the non-dressed ground state, cf figure 2(b). Along the axes ($X = 0$ or $Y = 0$), on the other hand, $E^{(2)}_{\kappa}(\mathbf{R})$ vanishes and the non-dressed Rydberg and ground state energy surfaces coincide. As a consequence, the continuous azimuthal symmetry of the two-dimensional ground state trapping potential is reduced to a fourfold one, see figure 2(a).

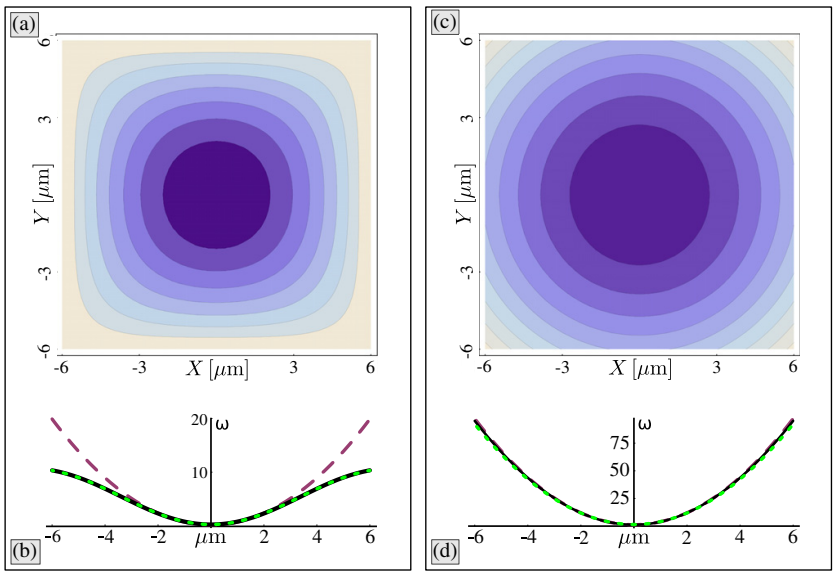

Figure 2. (a) Contour plot of the dressed ground state trapping potential for $B = 25\,\mathrm{G}$, $G = 2.5\,\mathrm{Tm}^{-1}$, $\omega_{\mathrm{ps}}^{(0)} = 2\pi \times 100\,\mathrm{MHz}$, $\omega_{\mathrm{np}}^{(0)} = 2\pi \times 130\,\mathrm{MHz}$, $\Delta_1 = -2\pi \times 40\,\mathrm{GHz}$ and $\Delta_2 = -2\pi \times 1.5\,\mathrm{MHz}$. (b) Cut along the diagonal $X = Y$ of the same surface (solid line); the short-dashed line which is on top of the solid black curve corresponds to the analytical solution (22) of the simplified three-level system. For comparison, the cut along the axis $X = 0$—where $E_{40\mathrm{S}}^{(2)}(\mathbf{R})$ does not contribute—is also illustrated, which corresponds to the trapping potential $E_{5\mathrm{S}}(\mathbf{R})$ of the ground state (dashed line). (c), (d) Same as in (a) and (b), respectively, but for $B = 1\,\mathrm{G}$. In this case, all three curves coincide on the scale of (d). The energy scale of all subfigures is given by the ground state trap frequency $\omega = \sqrt{G^2/MB}$.

In addition to the full numerical solution, in figure 2(b) the results of the simplified three-level scheme according to (22) are illustrated as well (short-dashed line). Since in the Ioffe field dominated regime the spatial variation of the quantization axis is minor, (22) agrees very well with the solution of the full 32-level problem (solid line). This allows us to recapitulate the above-made observations on grounds of the analytical expressions available within the reduced level scheme. For this reason, let us first consider the single-photon Rabi frequencies as given by (16) and (17). Because of the strong Ioffe field, they experience only a weak spatial dependence and are therefore essentially defined by their values $\omega_{\mathrm{ps}}^{(0)}$ and $\omega_{\mathrm{np}}^{(0)}$ at the origin. As a consequence, also the light shifts V_n and V_s (cf (20) and (21)) as well as the effective two-photon Rabi frequency Ω (cf (19)) can be approximated by their values at the origin. Hence, these quantities are not contributing to the particular shape of the dressed ground state energy surface. Omitting in this manner all contributions from (23) that merely yield a constant energy offset, one arrives at

$$E_-(\mathbf{R}) = \tilde{E}_{5\mathrm{S}}(\mathbf{R}) + \frac{\Omega^2}{4\Delta_2^2} E_{40\mathrm{S}}^{(2)}(\mathbf{R}) + \mathrm{const.} \tag{24}$$

That is, the deviation of the dressed ground state surface from its non-dressed counterpart is given by

$$E_-(\mathbf{R}) - E_{5\mathrm{S}}(\mathbf{R}) = \frac{\Omega^2}{4\Delta_2^2} E_{40\mathrm{S}}^{(2)}(\mathbf{R}). \tag{25}$$

This complies with the observations made before: $E_\kappa^{(2)}(\mathbf{R})$ possesses the envisaged discrete azimuthal symmetry (C_{4v}) and contributes mostly close to the diagonals of the two-dimensional trapping surface while vanishing on the axes. Moreover, $E_{40\mathrm{S}}^{(2)}(\mathbf{R}) < 0$ which agrees with the lowering of the energy surface. Hence, the regime of strong Ioffe fields in combination with a strong laser coupling allows us to map the specific features of the Rydberg trapping potential onto the ground state.

In figures 2(c) and (d) the same dressed trapping potential as before is illustrated, but now for $B = 1\,\mathrm{G}$. The reduction of the Ioffe field strength has basically two effects. First of all, considering the same spatial range as before the variation of the quantization axis is stronger. Consequently, the simplified three-level approach starts to slightly deviate from the exact solution, as can be observed in figure 2(d). Secondly, decreasing the Ioffe field influences the dressed potential by altering the Rydberg surface. For $B = 1\,\mathrm{G}$, $G = 2.5\,\mathrm{Tm}^{-1}$, the Rydberg trapping potential is not quite as shallow as for $B = 25\,G$, $G = 2.5\,\mathrm{Tm}^{-1}$ and now supports a few confined centre of mass states [23]. Consequently, the deviation between the Rydberg and the ground state surface is not as strong as in the previous case, resulting in a reduced lowering of the energy surface along the diagonal. Considering the two-dimensional trapping potential, the azimuthal symmetry is thus nearly recovered. In view of (24) this can be understood as follows. While the contribution $E_{40\mathrm{S}}^{(2)}(\mathbf{R})$ is identical for both cases (it depends only on the magnetic field gradient G rather than on the Ioffe field strength B), the spatial dependence of $E_{5\mathrm{S}}(\mathbf{R})$ is stronger in the case of the weaker Ioffe field. Hence, for a decreasing Ioffe field the importance of $E_{40\mathrm{S}}^{(2)}(\mathbf{R})$ is diminished and the original behaviour of the ground state trapping potential $E_{5\mathrm{S}}(\mathbf{R})$ is more and more recovered. Note that this does *not* imply a smaller contribution of the Rydberg level to the dressed state. This regime is thus particularly useful if any change of the trapping surface due to the Rydberg dressing is not desirable but the admixture of the Rydberg character is still required.

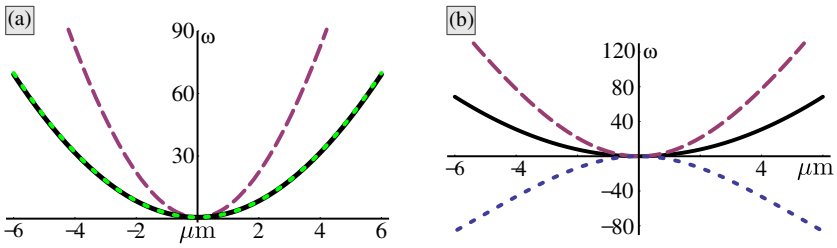

Figure 3. (a) Cut along the diagonal of the dressed ground state trapping potential for $B = 0.25$ G, $G = 2.5\,\mathrm{Tm}^{-1}$, $\omega_{\mathrm{ps}}^{(0)} = 2\pi \times 750$ MHz, $\omega_{\mathrm{np}}^{(0)} = 2\pi \times 100$ MHz, $\Delta_1 = -2\pi \times 75$ GHz and $\Delta_2 = -2\pi \times 5$ MHz. Note that in this strong gradient regime the trapping potential shows a continuous azimuthal symmetry; hence the corresponding contour plot is not provided. The trap frequency of the dressed surface (solid line) is greatly reduced compared to the trapping potential $E_{5\mathrm{S}}(\mathbf{R})$ of the ground state (dashed line). Turning off the second laser, i.e. setting $\omega_{\mathrm{np}}^{(0)} = 0$ hardly changes the shape of the potential surface (short-dashed line, on top of the black solid curve). (b) Spatially dependent light shift (short-dashed line) that in combination with the energy surface of the ground state (dashed line) leads to the trapping potential presented in (a) (solid line). The energy scale of all subfigures is given by the ground state trap frequency $\omega = \sqrt{G^2/MB}$.

Regarding the magnetic field parameters, the previous example represents the intermediate regime between the Ioffe dominated and the gradient dominated case; the latter let us investigate in the following. To achieve a strong gradient Ioffe–Pritchard configuration, we further reduce the Ioffe field to $B = 0.25\,\mathrm{G}$ and leave the magnetic field gradient $G = 2.5\,\mathrm{Tm}^{-1}$ unchanged. An important aspect of the strong gradient regime is the contribution of $E_{40\mathrm{S}}^{(2)}(\mathbf{R})$ to the dressed ground state energy surface. Already in the case of figures 2(b) and (d) it was indicated that the influence of $E_{40\mathrm{S}}^{(2)}(\mathbf{R})$ is diminished if the gradient field becomes more important. Indeed, for the present field parameters the deviation of the Rydberg trapping potential from the ground state potential is minor and many centre of mass states can be confined. Thus, in the spatial domain we are considering, the continuous azimuthal symmetry of the ground state trapping potential is conserved and we present in figure 3 only cuts along the diagonal of the dressed ground state energy surface. The parameters of the lasers are $\omega_{\mathrm{ps}}^{(0)} = 2\pi \times 750$ MHz, $\omega_{\mathrm{np}}^{(0)} = 2\pi \times 100\,\mathrm{MHz}$, $\Delta_1 = -2\pi \times 75\,\mathrm{GHz}$ and $\Delta_2 = -2\pi \times 5$ MHz.

The dashed line in figure 3(a) represents the non-dressed ground state trapping potential, $E_{5\mathrm{S}}(\mathbf{R})$. As one can observe, the two-photon dressing (solid line) substantially alters this surface by significantly reducing the trap frequency, namely, from $2\pi \times 638$ to $2\pi \times 381$ Hz. Although the simplified three-level system derived in section 4 is not able to reproduce this result quantitatively, it nevertheless provides us a qualitative understanding of the underlying physics, as we shall demonstrate in the following. In the case of a strong gradient field, the light shift V_s experienced by the ground state atom, (21), shows a strong spatial dependence and therefore cannot be omitted in (23). Specifically, it can be approximated for small centre of mass coordinates by

$$V_s \approx V_s^{(0)} \cdot \left(1 - \frac{1}{2}\frac{G^2\rho^2}{B^2}\right), \tag{26}$$

where $V_s^{(0)} = -\frac{1}{4}\frac{|\omega_{ps}^{(0)}|^2}{\tilde{E}_p - \tilde{E}_s + \Delta_1}$ denotes the light shift at the origin. Except for constant contributions, the dressed ground state surface then reads

$$E_-(\mathbf{R}) \propto E_{5\mathrm{S}}(\mathbf{R}) - \frac{1}{2}\frac{G^2\rho^2}{B^2}V_s^{(0)} \tag{27}$$

$$= \frac{1}{2}M\left(\omega^2 - \frac{G^2}{MB^2}V_s^{(0)}\right)\rho^2, \tag{28}$$

i.e. one encounters a reduced trap frequency $\tilde{\omega}^2 \equiv \omega^2 - \frac{G^2}{MB^2}V_s^{(0)}$. Note that the azimuthal symmetry of $E_-(\mathbf{R})$ is conserved; hence the dressed trapping potentials experienced in this regime are qualitatively different from the one of figures 2(a) and (b). We stress that (27) only serves for our qualitative understanding of the underlying physics. In the given regime, it fails to quantitatively reproduce the dressed potentials. The actual spatial dependence of the light shift is illustrated as the short-dashed line in figure 3(b). It has been calculated by solving the full 32-level system but without the contribution of the Ioffe–Pritchard trapping potentials. The combination with the confinement $E_{5\mathrm{S}}(\mathbf{R})$ (dashed line) finally yields the surface of a reduced trap frequency (solid line).

The short-dashed line in figure 3(a) represents the trapping potential for $\omega_{\mathrm{np}}^{(0)} = 0$, i.e. in the absence of the second laser that couples to the Rydberg state. Remarkably, turning off the second laser hardly changes the dressed potential. Hence, for the given example it is the interplay between the spatially varying quantization axis of the Ioffe–Pritchard field and the fixed polarization of the first laser that determines the spatially dependent light shift. As in the case of figures 2(c) and (d), this does not mean that the Rydberg state does not contribute to the dressed state. Hence, in the strong gradient regime we have two means to manipulate a ground state atom: with the first laser, one can alter the trapping potential experienced by the dressed atom and with the second laser we can in addition admix some Rydberg character to the atomic wavefunction.

The configuration leading to figure 3 has one drawback: since the influence of the spatial-dependent light shift on the trapping potential strongly depends on the coupling strength to the intermediate state, the effective lifetime of the dressed state is restricted. The issue of the finite lifetime is discussed in more detail in section 5.3. For now, let us remark that for the particular case of figure 3, a lifetime of $\approx$1 ms can be achieved. Hence, the proposed scheme is suitable for the scenarios where a short-term manipulation of the trapping potential is needed, e.g. for the modulation of the trap frequency on short timescales.

5.2. Dressed trapping potentials of the $m_F = 0$ state

In the above discussion, we focused on the dressed ground state arising from the $m_F = 2$ magnetic sublevel of the $5S_{1/2}$, $F = 2$ electronic state. Since ultracold samples of ground state atoms can nowadays be routinely prepared and magnetically trapped in this state, this is a sensible choice. Nevertheless, also different magnetic sublevels merit a closer look. As an example, we consider in the following dressed states of the $m_F = 0$ state. Note that the latter is untrapped in a pure Ioffe–Pritchard trap, i.e. without the coupling lasers. Therefore, one can expect that the influence of the specific features of the Rydberg trapping potential on the shape of the dressed surface is much more pronounced than in the case of the $m_F = 2$ dressed state. Both examples that are presented in the following belong to the strong gradient regime where the simplified three-level scheme is no longer valid and the full 32 level system must be considered.

In figures 4(a) and (b) the trapping potential of the dressed $m_F = 0$ ground state atom is illustrated for the configuration $B = 1\,\mathrm{G}$, $G = 10\,\mathrm{Tm}^{-1}$, $\omega_{\mathrm{ps}}^{(0)} = 2\pi \times 100\,\mathrm{MHz}$, $\omega_{\mathrm{np}}^{(0)} = 2\pi \times 35\,\mathrm{MHz}$, $\Delta_1 = -2\pi \times 14\,\mathrm{GHz}$ and $\Delta_2 = -2\pi \times 10\,\mathrm{MHz}$. The first thing to note is that—in contrast to the non-dressed $m_F = 0$ state—the atom experiences a confining potential that is due to the spatially dependent light shift of the off-resonant laser coupling. Moreover, figure 4(a) reveals the fourfold symmetry known from the Rydberg trapping potential $E_{40\mathrm{S}}(\mathbf{R})$. Because the admixed Rydberg surface has not to compete against a strong magnetic confinement of the ground state according to $\boldsymbol{\mu}_F \cdot \mathbf{B}(\mathbf{R})$, the anti-trapping effect of $E_{40\mathrm{S}}^{(2)}(\mathbf{R})$ becomes particularly visible in the dressed potential of the $m_F = 0$ state. In figure 4(b) the cut along the diagonal of the dressed potential is illustrated (solid line). As expected, the admixture of the Rydberg surface eventually changes the character of the trapping potential from confining to de-confining when going to larger centre of mass coordinates. However, for very large coordinates a weak confining behaviour is recovered that can be explained as follows. For such large centre of mass coordinates, the contribution $E_{40\mathrm{S}}^{(2)}(\mathbf{R})$ shifts the Rydberg state far off-resonant and thereby diminishes the contribution of the Rydberg level to the dressed state. The slightly confining character of the dressed potential in this regime is reminiscent of the spatially dependent light shift. Note that the azimuthally symmetric dressed potential arising in the absence of the second laser (short-dashed line) coincides very well with the two-photon dressed potential along the axes (dashed line). Hence, the first laser can be used to trap and prepare the atoms in the $m_F = 0$ ground state. By switching on the second laser, the Rydberg state gets admixed, resulting in the above-described significant change of the trapping potential in the vicinity of the diagonals ($X = Y$). Overall, the influence of the Rydberg surface is much more distinct than in the case of the $m_F = 2$ dressed states, cf figure 2.

For comparison, we show in figures 4(c) and (d) the dressed trapping potentials of the $m_F = 0$ state for a more dominant gradient field. The actual parameters are $B = 0.1\,\mathrm{G}$, $G = 10\,\mathrm{T\,m}^{-1}$, $\omega_{\mathrm{ps}}^{(0)} = 2\pi \times 150\,\mathrm{MHz}$, $\omega_{\mathrm{np}}^{(0)} = 2\pi \times 50\,\mathrm{MHz}$, $\Delta_1 = -2\pi \times 15\,\mathrm{GHz}$ and $\Delta_2 = -2\pi \times 10\,\mathrm{MHz}$. This configuration results in a much tighter confinement ($\omega = 2\pi \times 187\,\mathrm{Hz}$ compared to $\omega = 2\pi \times 25\,\mathrm{Hz}$ for the previous example) and a deeper trap along the diagonals. On the other hand, the revival of the weak trapping character as previously observed in figure 4(b) for large centre of mass coordinates along the diagonal is lost since the light shift of the first laser already reached a constant asymptotic behaviour in this regime. As discussed for the previous example, the contribution $E_{40\mathrm{S}}^{(2)}(\mathbf{R})$ shifts the Rydberg state far off-resonant and thereby diminishes the influence of the second laser on the excitation dynamics. Consequently, for large centre of mass coordinates close to the diagonal the dressed surface approaches the asymptotic of the single-photon dressing of the first laser (short-dashed line in figure 4(d)). In contrast, along the axes (dashed line) the potential does not reach a constant asymptote but maintains a weak confining behaviour. The latter is due to the admixture of predominantly $m_j = 1/2$ Rydberg states: since we assumed the two-photon transition to be blue-detuned, the magnetic field interaction $\propto m_j |\mathbf{B}(\mathbf{R})|$ pushes the $m_j = 1/2$ Rydberg state closer to resonance and in the same manner repels its $m_j = -1/2$ counterpart. Hence, the dressed state shows a stronger admixture of trapped than anti-trapped Rydberg states, giving rise to a confining energy surface. We remark that not only the Rydberg state contributes to the dressed state. In fact, the first laser slightly mixes the $5S_{1/2}$, $F = 2, m_F = 0$ state with $m_F \neq 0$ states of the same hyperfine level. However, the $m_F < 0$ states are admixed in the same degree as their $m_F > 0$ counterparts such that their confining and de-confining characters cancel.

We remark that, as in the case of figure 3, the effective lifetime of the dressed $m_F = 0$ states is restricted to a few ms due to the coupling to the intermediate state. The latter is required for the confining light-shift potential of the otherwise untrapped $m_F = 0$ state.

5.3. Experimental issues

Let us finish by commenting on the experimental feasibility of the above-discussed scheme. The proposed dressed states possess a finite lifetime due to the spontaneous decay of the Rydberg state. The associated effective lifetime can be estimated by

$$\tau = \frac{\tau_n}{|c_n|^2}, \tag{29}$$

with c_n being the admixture coefficient of the Rydberg state; within the simplified three-level scheme it evaluates to $|c_{n,3\mathrm{l}}|^2 = [\Omega/2\tilde{\Delta}_2]^2$ with $\tilde{\Delta}_2 = \Delta_2 + V_n - V_s + E_{\mathrm{hfs}}$. τ_n denotes the radiative lifetime of the $nS_{1/2}$ Rydberg atom and can be parametrized as $\tau_n = \tau'(n-\delta)^\gamma$ where one finds $\tau' = 1.43$ ns and $\gamma = 2.94$ for $l = 0$, $\tau' = 2.76$ ns and $\gamma = 3.02$ for $l = 1$, and $\tau' = 2.09$ ns and $\gamma = 2.85$ for $l = 2$ [33]. For the $40S_{1/2}$ Rydberg state, this yields $\tau_{40} = 58\,\mu\mathrm{s}$. In table 1, the effective lifetimes for the examples presented in this work are tabulated. Because the Rydberg state is only weakly admixed ($|c_n|^2 < 10^{-2}$ for all examples), effective lifetimes greater than 10 ms are obtained. Besides the finite lifetime of the Rydberg state, one needs in addition to account

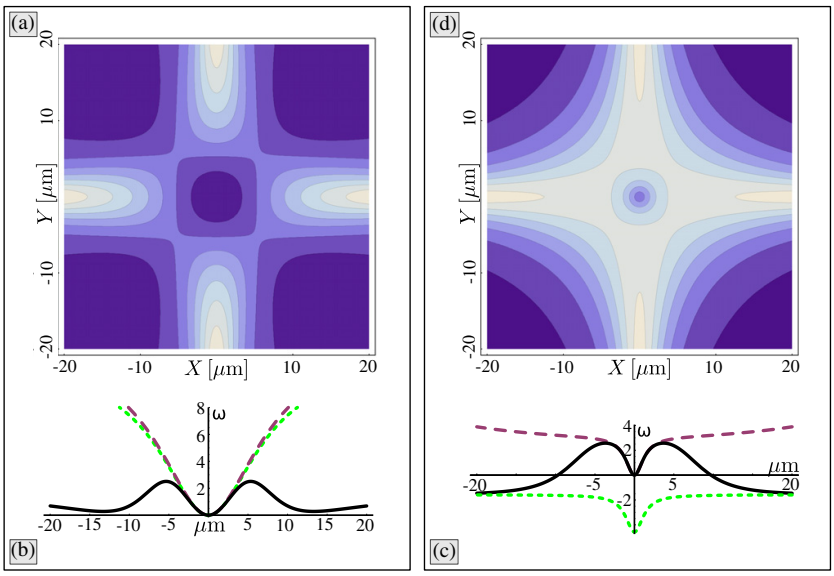

Figure 4. (a) Contour plot of the dressed ground state trapping potential for the $5S_{1/2}$, $m_F = 0$ state. The parameters are $B = 1$ G, $G = 10\,\mathrm{Tm}^{-1}$, $\omega_{\mathrm{ps}}^{(0)} = 2\pi \times 100$ MHz, $\omega_{\mathrm{np}}^{(0)} = 2\pi \times 35$ MHz, $\Delta_1 = -2\pi \times 14$ GHz and $\Delta_2 = -2\pi \times 10$ MHz. (b) Cut along the diagonal $X = Y$ (solid line) and along the axis with $X = 0$ (dashed line) of the same surface; the short-dashed line corresponds to the single-photon dressing, i.e. $\omega_{\mathrm{np}}^{(0)} = 0$. For comparison, all curves are offset to zero at the origin. (c), (d) Same as in subfigures (a) and (b), respectively, but for $B = 0.1$ G, $G = 10\,\mathrm{Tm}^{-1}$, $\omega_{\mathrm{ps}}^{(0)} = 2\pi \times 150$ MHz, $\omega_{\mathrm{np}}^{(0)} = 2\pi \times 50$ MHz, $\Delta_1 = -2\pi \times 15$ GHz and $\Delta_2 = -2\pi \times 10$ MHz. In subfigure (d) we refrained from offsetting all curves to zero at the origin but rather applied a common offset such that the joint asymptote of the solid and dotted line becomes evident. Note that the detunings are defined in the same way as for the $5S_{1/2}$, $m_F = 2$ case. The energy scale in all subfigures is given in terms of the trap frequency. The latter has been gained by a harmonic fit around the origin, yielding $\omega = 2\pi \times 25$ Hz and $\omega = 2\pi \times 187$ Hz for the first and second configuration, respectively.

Table 1. Effective lifetimes of the dressed states considered in this section. The lifetimes are determined according to (29) using the Rydberg admixture coefficient c_n of the full 32-level system. When applicable, the admixture coefficient $c_{n,3l}$ of the simplified three-level system is provided for comparison. In addition, the admixture coefficient c_p of the intermediate state and the resulting lifetime are given.

Configuration	$\lvert c_{n,3l}\rvert^2$	$\lvert c_n\rvert^2$	τ_n(ms)	$\lvert c_p\rvert^2$	τ_p(ms)
Figure 2(a)	0.004 186	0.004 134	14.0	1.83×10^{-6}	14.2
Figure 2(c)	0.004 533	0.004 472	13.0	1.84×10^{-6}	14.1
Figure 3(a)	–	0.001 433	40.5	25.2×10^{-6}	1.03
Figure 4(a)	–	0.000 040	1457	12.8×10^{-6}	2.03
Figure 4(c)	–	0.000 154	377	25.2×10^{-6}	1.03

for the decay of the intermediate $5P_{3/2}$ level that possesses a much shorter radiative lifetime of $\tau_p = 26$ ns. The resulting effective lifetimes together with the coupling coefficients are provided in table 1 as well. As it turns out, the decay of the intermediate state constitutes the dominating loss channel, allowing for lifetimes $\gtrsim$1 ms.

The resulting lifetimes need to be compared with the timescales emerging in actual experiments. In case of figure 2(a), it is desirable to map the dressed potential by the external motion. Given the trap frequency of $\omega = 2\pi \times 63.8$ Hz, this yields a timescale of about 15 ms which is of the same order of magnitude as the effective lifetime. For the remaining examples addressed in this work, the effective lifetime is not quite sufficient to cover the timescale of the external motion. Hence, in these cases the proposed scheme is more suitable whenever only a short-term manipulation of the trapping potential is required. Finally, we remark that the effective lifetime can be further prolonged by coupling to Rydberg states with a higher principle quantum number n and by substituting the intermediate $5P_{3/2}$ state by a more long-lived one such as the $6P_{3/2}$ state.

Similar to the effective lifetime, the van der Waals interaction of two Rydberg atoms is suppressed by $\lvert c_n\rvert^4$. The latter interaction results in an energy shift Δ_{vdW} that depends on the interparticle distance and effectively alters the detuning of the two-photon transition. In order to avoid any such effects, Δ_{vdW} should be well below the excitation detuning Δ_2. Taking $c_n = 0.1$ and $\Delta_{\mathrm{vdW}} < 2\pi \times 0.1$ MHz as an (quite restrictive) example yields a minimum interparticle distance of $\approx$1 μm.

6. Summary

In the present work, we investigated a magnetically trapped rubidium atom that is coupled to its nS Rydberg state via a two-photon laser transition. We studied the off-resonant case where the ground state atom becomes *dressed* by the Rydberg state and vice versa. By this procedure, the peculiar properties of Rydberg atoms become accessible also for ground state atoms. In particular, we explored how the trapping potential experienced by a ground state atom in a magnetic Ioffe–Pritchard trap can be manipulated by means of such an off-resonant laser coupling. It is demonstrated that in the limit of a strong offset field the fourfold azimuthal symmetry, which is inherent for the trapping potential of the Rydberg atom, is mirrored in the dressed ground state trapping potential. In this regime, a simplified three-level scheme

is derived that facilitates the interpretation of the observed results. In the opposite regime of a strong gradient, the delicate interplay between the spatially varying quantization axis of the Ioffe–Pritchard field and the fixed polarizations of the laser transitions greatly influences the actual shape of the dressed trapping potentials. In this manner, the trapping potentials of ground state atoms can be manipulated substantially.

Acknowledgments

This work was supported by the German Research Foundation (DFG) within the framework of the Excellence Initiative through the Heidelberg Graduate School of Fundamental Physics (GSC 129/1). MM acknowledges financial support from the Landesgraduiertenförderung Baden-Württemberg. Financial support from the DFG through the grant Schm 885/10-3 is gratefully acknowledged.

Appendix

In this appendix the two-level Hamiltonian (18) is derived. Within the rotating wave approximation [34] our initial, time-independent Hamiltonian in the simplified three-level scheme reads

$$\mathcal{H}_{\mathrm{rwa}} = \underbrace{\begin{pmatrix} \Delta_1 + \tilde{E}_p & 0 & 0 \\ 0 & \Delta_2 + \tilde{E}_n + E_{\mathrm{hfs}} & 0 \\ 0 & 0 & \tilde{E}_s \end{pmatrix}}_{\equiv \mathcal{H}_0} + \underbrace{\begin{pmatrix} 0 & \frac{\omega_{\mathrm{pn}}}{2} & \frac{\omega_{\mathrm{ps}}}{2} \\ \frac{\omega_{\mathrm{np}}}{2} & 0 & 0 \\ \frac{\omega_{\mathrm{sp}}}{2} & 0 & 0 \end{pmatrix}}_{\equiv \mathcal{V}}. \tag{A.1}$$

Here, $\tilde{E}_n \equiv \frac{1}{2}|\mathbf{B}(\mathbf{R})| + C \cdot G^2X^2Y^2$, $\tilde{E}_s \equiv \frac{1}{2}|\mathbf{B}(\mathbf{R})|$ and $\tilde{E}_p \equiv |\mathbf{B}(\mathbf{R})|$ are the trapping potentials of the individual energy levels and E_{hfs} includes the energy shift due to the hyperfine splitting of the Rydberg state as well as the Zeeman shift of the nuclear spin. The laser detunings are defined by $\Delta_1 = E_p^{\mathrm{el}} - E_s^{\mathrm{el}} - \omega_1$ and $\Delta_2 = E_n^{\mathrm{el}} - E_s^{\mathrm{el}} - \omega_1 - \omega_2$. The second term, $\mathcal{V}$, represents a perturbation that couples the 'model space' $\{n, s\}$ consisting of the $n\mathrm{S}_{1/2}$ Rydberg and the $5\mathrm{S}_{1/2}$, $F = m_F = 2$ ground state via the single-photon Rabi frequencies ω_{ps} and ω_{np}, cf (16)–(17), to the one-dimensional orthogonal subspace $\{p \equiv 5\mathrm{P}_{3/2}, F = m_F = 3\}$ of the intermediate level.

We are considering the regime where the intermediate level p is only weakly coupled to both the ground state s and the Rydberg level n. Such a scenario allows us to adiabatically eliminate the intermediate state p from the excitation dynamics. Specifically, if $|\Delta_1| \gg \omega_{\mathrm{ps}}$ and $|\Delta_1 - \Delta_2| \gg \omega_{\mathrm{np}}$, quasidegenerate van Vleck perturbation theory provides us a unitary transformation e^{-G} that block diagonalizes $\mathcal{H}_{\mathrm{rwa}}$ [32]. In this manner, the subspace $\{p\}$ is decoupled from the dynamics of the model space $\{n, s\}$, yielding an effective Hamiltonian $H_{2l} = H_0 + W$ for the latter. Our goal is to determine the unitary transformation e^{-G} and hence the effective interaction W within the model space $\{n, s\}$.

The formalism to calculate G and accordingly W is derived in [32], which we briefly summarize for our system in the following. As shown in (A.1), the Hamiltonian H_{rwa} can be divided into a zero-order part H_0 and a perturbation V with the zero-order eigenfunctions $H_0|t\rangle = \varepsilon_t|t\rangle$. The set of eigensolutions of H_0 can be partitioned into two subsets $\{t, u, \ldots\} = \{\alpha, \beta, \ldots\} \cup \{i, j, \ldots\}$, defining the model space $\{\alpha, \beta, \ldots\} = \{n, s\}$ and its orthogonal complement $\{i, j, \ldots\} = \{p\}$. The projection operator into the model space and its orthogonal complement read $P = |n\rangle\langle n| + |s\rangle\langle s|$ and $Q = 1 - P = |p\rangle\langle p|$, respectively. Any operator A can be partitioned into a block diagonal part A_D and a block off-diagonal part A_X, $A = A_D + A_X$. In our case, the perturbation V only possesses block off-diagonal matrix elements, i.e. $V_D = 0$ and we find $H_D = H_0$ and $H_X = V_X$.

Within the canonical form of van Vleck perturbation theory, we require $G = G_X$, i.e. $G_D = 0$ for the operator determining the unitary transformation e^{-G}. Moreover, G is an anti-Hermitian operator, $G = -G^\dagger$. It is defined order by order via

$$[H_0, G^{(1)}] = -V_X, \tag{A.2}$$

$$[H_0, G^{(2)}] = -[V_D, G^{(1)}] = 0. \tag{A.3}$$

For higher orders, see [32]; the zeroth-order contribution vanishes, i.e. $G^{(0)} = 0$. The order-by-order computation of the effective interaction W is as follows:

$$W^{(1)} = V_D = 0, \tag{A.4}$$

$$W^{(2)} = \tfrac{1}{2}[V_X, G^{(1)}]. \tag{A.5}$$

Explicit equations for the $G^{(n)}$ can be gained from (A.2)–(A.3) using the resolvent formalism. In first order, one finds the matrix representation

$$\mathcal{G}^{(1)}_{j\alpha} = \frac{\mathcal{V}_{j\alpha}}{\varepsilon_\alpha - \varepsilon_j}. \tag{A.6}$$

Note that as per definition there are no block diagonal contributions, i.e. $\mathcal{G}^{(n)}_{\alpha\beta} = 0$. The second-order matrix elements of the effective interaction W correspondingly read

$$\mathcal{W}^{(2)}_{\beta\alpha} = \frac{1}{2}\sum_i \mathcal{V}_{\beta i}\mathcal{V}_{i\alpha}\left(\frac{1}{\varepsilon_\alpha - \varepsilon_i} + \frac{1}{\varepsilon_\beta - \varepsilon_i}\right) \tag{A.7}$$

$$= \frac{1}{8}\omega_{\beta p}\omega_{p\alpha}\left(\frac{1}{\varepsilon_\alpha - \varepsilon_p} + \frac{1}{\varepsilon_\beta - \varepsilon_p}\right). \tag{A.8}$$

Hence, the above-described procedure provides us an effective two-level system whose excitation dynamics are determined up to second order by the Hamiltonian

$$\mathcal{H}_{2l} = \mathcal{H}_0 + \mathcal{W}^{(2)} = \begin{pmatrix} \Delta_2 + \tilde{E}_n + E_{\mathrm{hfs}} + V_n & \Omega/2 \\ \Omega^*/2 & \tilde{E}_s + V_s \end{pmatrix}, \tag{A.9}$$

where the effective interaction between the ground state and Rydberg state is given by the two-photon Rabi frequency

$$\Omega = \frac{\omega_{\rm ps}\omega_{\rm np}}{4}\left[\frac{1}{\tilde{E}_s - \tilde{E}_p - \Delta_1} + \frac{1}{\tilde{E}_n - \tilde{E}_p + \Delta_2 - \Delta_1 + E_{\rm hfs}}\right]. \quad \text{(A.10)}$$

The contributions

$$V_s = -\frac{1}{4}\frac{|\omega_{ps}|^2}{\tilde{E}_p - \tilde{E}_s + \Delta_1}, \quad \text{(A.11)}$$

$$V_n = -\frac{1}{4}\frac{|\omega_{np}|^2}{\tilde{E}_p - \tilde{E}_n + \Delta_1 - \Delta_2 - E_{\rm hfs}} \quad \text{(A.12)}$$

are the light shifts of the ground state and Rydberg state, respectively, which stem from the off-resonant laser dressing of the individual single-photon transitions [35].

References

[1] Gallagher T F 1994 *Rydberg Atoms* (Cambridge: Cambridge University Press)

[2] Urban E, Johnson T A, Henage T, Isenhower L, Yavuz D D, Walker T G and Saffman M 2009 Observation of Rydberg blockade between two atoms *Nat. Phys.* **5** 110

[3] Gaëtan A, Miroshnychenko Y, Wilk T, Chotia A, Viteau M, Comparat D, Pillet P, Browaeys A and Grangier P 2009 Observation of collective excitation of two individual atoms in the Rydberg blockade regime *Nat. Phys.* **5** 115

[4] Jaksch D, Cirac J I, Zoller P, Rolston S L, Côté R and Lukin M D 2000 Fast quantum gates for neutral atoms *Phys. Rev. Lett.* **85** 2208

[5] Lukin M D, Fleischhauer M, Côté R, Duan L M, Jaksch D, Cirac J I and Zoller P 2001 Dipole blockade and quantum information processing in mesoscopic atomic ensembles *Phys. Rev. Lett.* **87** 037901

[6] Saffman M and Mølmer K 2009 Efficient multiparticle entanglement via asymmetric Rydberg blockade *Phys. Rev. Lett.* **102** 240502

[7] Müller M, Lesanovsky I, Weimer H, Büchler H P and Zoller P 2009 Mesoscopic Rydberg gate based on electromagnetically induced transparency *Phys. Rev. Lett.* **102** 170502

[8] Olmos B, González-Férez R and Lesanovsky I 2009 Fermionic collective excitations in a lattice gas of Rydberg atoms *Phys. Rev. Lett.* **103** 185302

[9] Isenhower L, Urban E, Zhang X L, Gill A T, Henage T, Johnson T A, Walker T G and Saffman M 2010 Demonstration of a neutral atom controlled-NOT quantum gate *Phys. Rev. Lett.* **104** 010503

[10] Wilk T, Gaëtan A, Evellin C, Wolters J, Miroshnychenko Y, Grangier P and Browaeys A 2010 Entanglement of two individual neutral atoms using Rydberg blockade *Phys. Rev. Lett.* **104** 010502

[11] Santos L, Shlyapnikov G V, Zoller P and Lewenstein M 2000 Bose–Einstein condensation in trapped dipolar gases *Phys. Rev. Lett.* **85** 1791

[12] Pupillo G, Micheli A, Boninsegni M, Lesanovsky I and Zoller P 2010 Strongly correlated gases of Rydberg-dressed atoms: quantum and classical dynamics *Phys. Rev. Lett.* **104** 223002

[13] Cinti F, Jain P, Boninsegni M, Micheli A, Zoller P and Pupillo G 2010 A superfluid-droplet crystal and a free-space supersolid in a dipole-blockaded gas arXiv:1005.2403v3 [cond-mat.quant-gas]

[14] Henkel N, Nath R and Pohl T 2010 Three-dimensional roton excitations and supersolid formation in Rydberg-excited Bose–Einstein condensates *Phys. Rev. Lett.* **104** 195302

[15] Honer J, Weimer H, Pfau T and Büchler H P 2010 Collective many-body interaction in Rydberg dressed atoms arXiv:1004.2499v1 [cond-mat.quant-gas]

[16] Günther A, Kraft S, Kemmler M, Koelle D, Kleiner R, Zimmermann C and Fortágh J 2005 Diffraction of a Bose–Einstein condensate from a magnetic lattice on a microchip *Phys. Rev. Lett.* **95** 170405

[17] Singh M, Volk M, Akulshin A, Sidorov A, McLean R and Hannaford P 2008 One-dimensional lattice of permanent magnetic microtraps for ultracold atoms on an atom chip *J. Phys. B: At. Mol. Opt. Phys.* **41** 065301

[18] Gerritsma R, Whitlock S, Fernholz T, Schlatter H, Luigjes J A, Thiele J, Goedkoop J B and Spreeuw R J C 2007 Lattice of microtraps for ultracold atoms based on patterned magnetic films *Phys. Rev.* A **76** 033408

[19] Whitlock S, Gerritsma R, Fernholz T and Spreeuw R J C 2009 Two-dimensional array of microtraps with atomic shift register on a chip *New J. Phys.* **11** 023021

[20] Hezel B, Lesanovsky I and Schmelcher P 2006 Controlling ultracold Rydberg atoms in the quantum regime *Phys. Rev. Lett.* **97** 223001

[21] Hezel B, Lesanovsky I and Schmelcher P 2007 Ultracold Rydberg atoms in a Ioffe–Pritchard trap *Phys. Rev.* A **76** 053417

[22] Mayle M, Hezel B, Lesanovsky I and Schmelcher P 2007 One-dimensional Rydberg gas in a magnetoelectric trap *Phys. Rev. Lett.* **99** 113004

[23] Mayle M, Lesanovsky I and Schmelcher P 2009 Magnetic trapping of ultracold Rydberg atoms in low angular momentum states *Phys. Rev.* A **80** 053410

[24] Mayle M, Lesanovsky I and Schmelcher P 2009 Exploiting the composite character of Rydberg atoms for cold-atom trapping *Phys. Rev.* A **79** 041403

[25] Middelkamp S, Mayle M, Lesanovsky I and Schmelcher P 2010 Creating versatile atom traps by applying near-resonant laser light in magnetic traps *Phys. Rev.* A **81** 053414

[26] Marinescu M, Sadeghpour H R and Dalgarno A 1994 Dispersion coefficients for alkali-metal dimers *Phys. Rev.* A **49** 982

[27] Condon E U and Shortley G H 1935 *The Theory of Atomic Spectra* (Cambridge: Cambridge University Press)

[28] Li W, Mourachko I, Noel M W and Gallagher T F 2003 Millimeter-wave spectroscopy of cold Rb Rydberg atoms in a magneto-optical trap: quantum defects of the *n*s, *n*p and *n*d series *Phys. Rev.* A **67** 052502

[29] Armstrong L Jr 1971 *Theory of the Hyperfine Structure of Free Atoms* (New York: Wiley Interscience)

[30] Heidemann R, Raitzsch U, Bendkowsky V, Butscher B, Löw R, Santos L and Pfau T 2007 Evidence for coherent collective Rydberg excitation in the strong blockade regime *Phys. Rev. Lett.* **99** 163601

[31] Reetz-Lamour M, Amthor T, Deiglmayr J and Weidemüller M 2008 Rabi oscillations and excitation trapping in the coherent excitation of a mesoscopic frozen Rydberg gas *Phys. Rev. Lett.* **100** 253001

[32] Shavitt I and Redmon L T 1980 Quasidegenerate perturbation theories. A canonical van Vleck formalism and its relationship to other approaches *J. Chem. Phys.* **73** 5711

[33] de Oliveira A L, Mancini M W, Bagnato V S and Marcassa L G 2002 Measurement of Rydberg-state lifetimes using cold trapped atoms *Phys. Rev.* A **65** 031401

[34] Scully M O and Zubairy M S 1997 *Quantum Optics* (Cambridge: Cambridge University Press)

[35] Dalibard J and Cohen-Tannoudji C 1985 Dressed-atom approach to atomic motion in laser light: the dipole force revisited *J. Opt. Soc. Am.* B **2** 1707